

Advanced Generator Protection and Monitoring Using Transducer Measurements

Terry Foxcroft, *Snowy Hydro Limited, Australia*

Normann Fischer, Dale Finney, Satish Samineni, and Yu Xia, *Schweitzer Engineering Laboratories, Inc.*

Abstract—A number of generator issues are undetectable using the generator terminal voltage or current measurements. For example, a switching element failure in the exciter produces a characteristic harmonic signature in the field current. While some generator protective relays are capable of measuring the field current, the sampling rate may be insufficient to extract the relevant harmonics. Consider shaft current protection of hydroelectric generators. The measurement source is a shaft current transformer or Rogowski coil. The operating quantity is a fundamental or root mean square component, but the signal level will likely be too low for conventional current inputs to measure.

This paper reviews a number of generator protection and monitoring applications that use transducer measurements to complement current protection. The paper describes the factors that govern the signal characteristics. It defines the operating principles of the protection functions and the resulting transducer measurement requirements.

I. INTRODUCTION

This paper introduces new ideas and concepts that complement existing generator protection elements to provide better overall generator protection and monitoring. At present, by the time generator short-circuit protection operates, the generator has already sustained considerable damage, and the protection operation prevents only catastrophic generator failure from occurring. The protection algorithm and elements that we describe in this paper use transducer measurements to take the generator out of service before the generator sustains considerable damage. In addition, these measurements can alert the generator owner of an abnormal generator condition, so the owner can take the machine out of service in a controlled manner. This allows the generator to be repaired in a cost-effective and timely manner, thereby minimizing generator down time.

The IEEE Standards Dictionary [1] defines a transducer as “A device that converts energy from one domain into another. The device may be either a sensor or an actuator.” A sensor converts a physical quantity such as pressure or temperature into a signal that is suitable for processing by a monitoring, control, or protection device. The physical quantity could also be power system voltage or current. Therefore, voltage and current transformers (VTs and CTs) are also transducers, although often not considered as such.

Before discussing specific applications, we review some concepts associated with signal acquisition and processing. We show that the processing levels required to implement protection functions using transducer I/O are often similar to those required for conventional CT and VT quantities.

A. Isolation

A protective relay measures CT and VT secondary quantities. The CTs and VTs scale the primary quantities to values the relay can measure and also isolate the relay from the power system.

The situation is no different with transducer measurements. For example, generator field quantities will be in the range of hundreds of amperes and volts—well beyond the practical measurement range of a microprocessor-based relay. Field quantities could be scaled using current shunts and voltage divider networks. However, this would not provide isolation for the large amount of energy contained in the field circuit. A better solution is to derive these measurements using transducers placed close to the field circuit. When properly designed, these devices can provide thousands of volts of galvanic isolation and deliver a high-fidelity signal to the relay over a shielded, twisted-pair cable.

B. Scaling and Conversion Range

As is the case with CTs and VTs, it is important to select transducers that are sized appropriately for the measured quantity. The relay scaling function converts an input signal to an accurately scaled value while maintaining the integrity of the magnitude, phase, and offset. To provide this accuracy and remove any negative impacts of the conversion processes, some relays include optional gain, phase, and offset settings.

We can define the conversion range as the range of values that the input circuitry can resolve. The upper boundary of the conversion range is where the A/D converter (ADC) saturates and clipping begins to occur. Accuracy suffers when clipping occurs, but the measurement may still be useable. To find the lower boundary of the range, divide the range (determined by the designer) by 2^N , where N is the number of bits of the ADC. Usually, properly selecting the external transducer (similar to CT and VT selection) ensures an adequate measurement is available. In some applications, a wide conversion range may be important to ensure accurate measurement of both large and small signal levels.

C. Sampling Rate

The process of sampling converts the signal from the continuous to the discrete time domain. We can define a band-limited signal as one that can be decomposed into a finite number of frequency components. The Nyquist theorem states that a signal must be sampled at a minimum of twice

the highest frequency component of interest. Frequency components beyond this limit are “folded back” after sampling and appear as a lower frequency component in a process known as aliasing. For example, assume that an input containing a 1.1 kHz signal is sampled at 2 kHz. The 1.1 kHz component appears as a 0.9 kHz component in the frequency spectrum of the sampled waveform. For this reason, an analog low-pass (anti-aliasing) filter with a cutoff (corner) frequency of one-half the sampling frequency or lower must be applied prior to sampling.

D. Digital Filtering

For certain applications, it may be feasible to use the instantaneous value of a measurement. Generally, however, measurements are filtered first. Various parameters can be used to describe the characteristics of a filter both in the frequency and time domains. These include band-pass ripple, roll-off, time constant, and overshoot, to name a few. It is critical to apply the correct filter for the application. Some filters pass a range of frequencies as Fig. 1 shows.

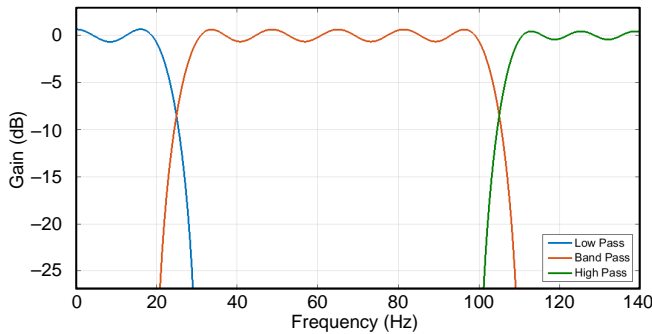


Fig. 1. Frequency response of low-, band-, and high-pass filters.

Other filters target a specific frequency and its harmonic components. For example, the cosine filter has a unity gain at the fundamental frequency and rejects dc as well as harmonics. The filter doesn’t completely reject interharmonics and subharmonics as Fig. 2 shows.

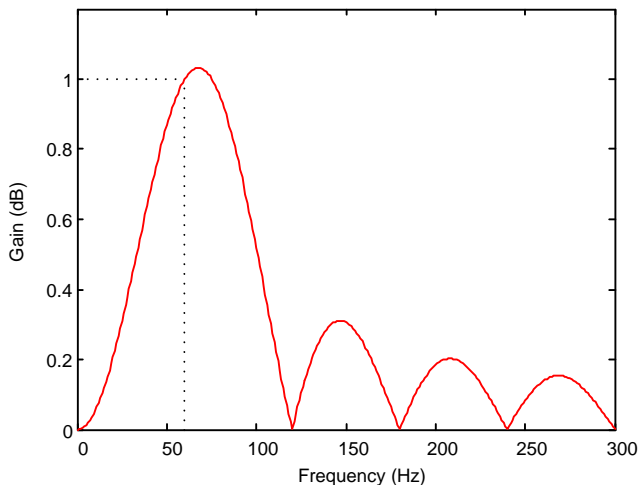


Fig. 2. Frequency response of a full-cycle cosine filter.

An RMS filter has a unity gain at the fundamental frequency, at dc, and at each harmonic. However, this filter

also measures interharmonics and subharmonics, but at these frequencies, it under- and overestimates the current magnitude as shown by the red current envelope in Fig. 3.

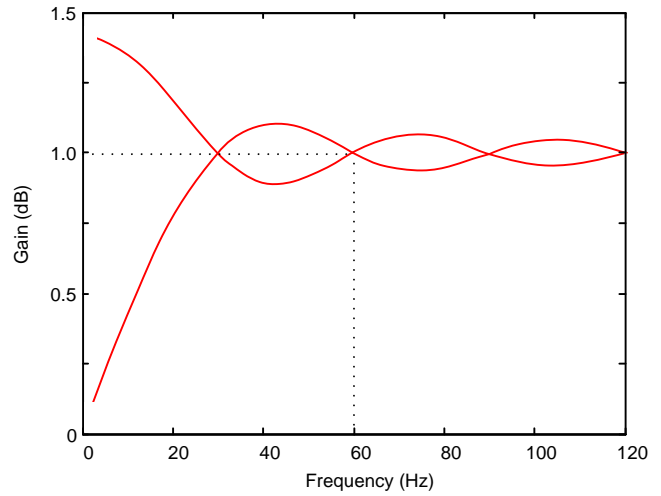


Fig. 3. Frequency response of a full-cycle RMS filter.

Another quantity of interest is the dc component. Traditionally, we derive this using a low-pass filter. Depending on the chosen corner frequency, the low-pass filter trades off a time-domain response for a high-frequency rejection. Another way to extract dc is to take an average of the samples over one period of the fundamental frequency. We can refer to this as a full-cycle dc filter. This calculation will ramp to the dc value in one cycle. It also rejects the fundamental and harmonic components.

In some applications, the frequency component of interest will be constant. For example, the natural frequencies of the generator shaft are dependent on the physical properties of the generator. In other applications, the frequency component of interest may not be constant. For example, the frequency components in the field current or shaft current vary with the generator frequency.

We calculate full-cycle filters, such as the cosine, RMS, and full-cycle dc filters, over a fixed number of samples or a window. When the window length matches the period of the signal, the gains will be as described previously. If the frequency of the signal changes and we don’t adjust the window length accordingly, the filter becomes less accurate. For example, the cosine filter of Fig. 2 has a window size equal to one power system cycle (1/60 Hz). If the signal frequency is slightly higher, the filter will overestimate the magnitude. In addition, the filter will not fully reject any harmonics at that frequency. One way to address this issue is to adjust the sampling rate as the frequency changes, such that the filter window and the signal period are always the same. This process is known as frequency tracking. Adjusting the sampling rate also impacts a band-pass filter. Depending on the application, this may not be desirable.

II. FIELD CURRENT AND VOLTAGE MONITORING FIELD MEASUREMENTS

We can implement a number of generator monitoring and protection functions using field measurements. As mentioned in Section I, transducers are required to provide suitable scaling. Shunts and voltage divider networks could be used but will not provide suitable isolation. Hall-effect transducers can provide scaling and isolation and have a wide frequency response down to the dc level.

A. Field Overload

As with any electric circuit, an overload can quickly cause serious damage to the field winding. The field winding, therefore, requires protection. IEEE C37.102 [2] specifies the thermal capability of the rotor as shown in Fig. 4. An inverse time curve can be implemented in a protective relay to coordinate with the thermal curve of the generator field. The input transducer must be scaled for the highest expected current magnitude. An RMS filter will provide the most accurate heating measurement. The IEEE standard recognizes that the thermal capability limits may be exceeded but that the number of such occurrences should not be more than twice a year.

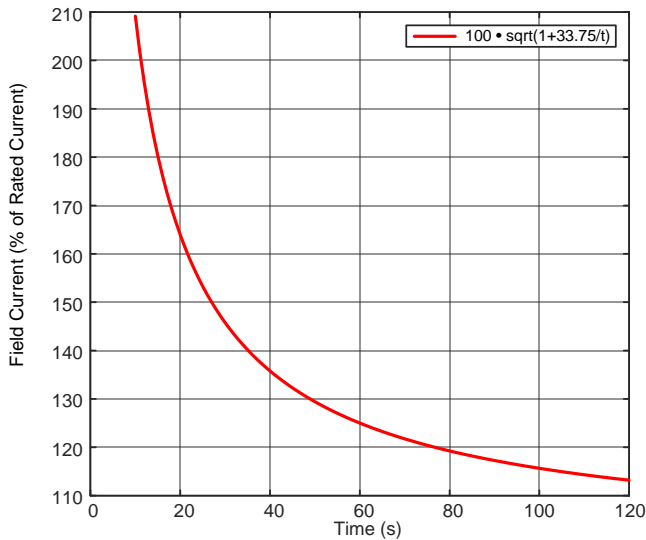


Fig. 4. Cylindrical rotor thermal capability [3].

B. Field Overtemperature

Even without an overload, a cooling failure can push the field winding temperature beyond its design rating. Direct measurement of the field temperature is not practical; however, we can indirectly measure the field temperature through real-time measurement of the field winding resistance. The winding resistance is in turn derived from the dc components of field voltage (V_{F_DC}) and field current (I_{F_DC}). The voltage drop across the field brushes will be in the range of 2 to 4 volts and can therefore impact the accuracy of the measurement. We can reconcile this voltage drop using a calibration setting (V_{BRUSH}). Application of this method requires an accurate measurement of brush voltage. This can be achieved during commissioning by making a second measurement of field voltage using a set of brushes

that don't carry current. The difference between the two measurements is the brush voltage. By measuring the ambient resistance (R_{AMB}) at ambient temperature (T_{AMB}), we can calculate the field temperature (T_{FIELD}) as follows [4]:

$$T_{FIELD} = T_{AMB} + \left(\frac{V_{F_DC} - V_{BRUSH}}{I_{F_DC} \cdot R_{AMB}} - 1 \right) \cdot \frac{1}{\alpha} \quad (1)$$

where:

α = resistive temperature coefficient of the field winding

The field winding temperature should not be calculated unless both V_{F_DC} and I_{F_DC} are within their operating range. In order to achieve a stable temperature indication, both the field voltage and current must be adequately filtered to remove harmonic components.

C. Exciter Problems

The previous two functions focused on the field winding. We can also use field measurements to identify problems in the exciter. For example, under normal operation, the dc output current of a six-pulse controlled rectifier will contain the 6th, 12th, 18th harmonics, etc. However, if a thyristor is either open or short circuited, the exciter output current will also include the fundamental plus additional harmonics. Fig. 5 shows the main components of the exciter current following a thyristor open-circuit event occurring at time equal to one second. Note the significant increase in the fundamental and second harmonic.

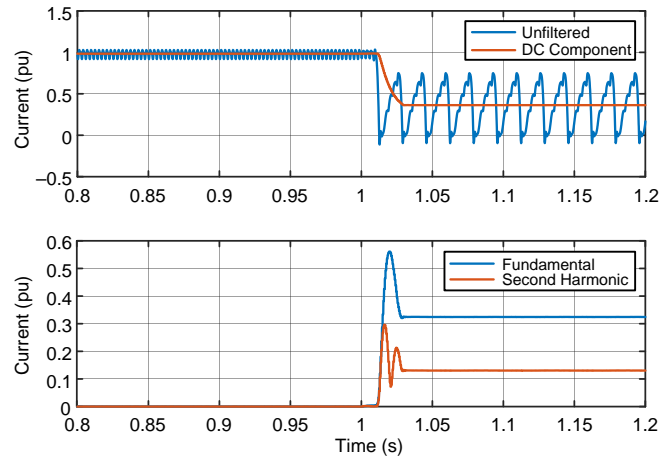


Fig. 5. Six-pulse converter with an open thyristor.

However, transient currents in the stator winding will also induce transient currents into the field winding. Specifically, a dc current in the stator winding will produce a fundamental current (I_{F_FUND}) in the field (assuming the generator is at rated speed). Fig. 6 shows the harmonic current content of the field current following a phase-to-ground fault at the generator step-up unit (GSU) transformer high-voltage terminal. Note that both the fundamental and second harmonic are present on initiation of the fault but the fundamental dies out. The dc offset in the stator current is a function of the system X/R ratio and can be significant at the generator.

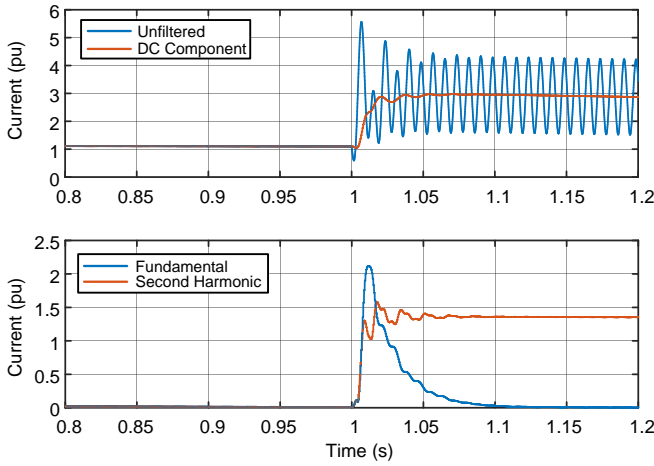


Fig. 6. Field current during a phase-to-ground fault at the GSU high-voltage terminals.

One solution to secure the element for an external fault would be to delay operation for a period longer than the expected duration of the fundamental transient. Fortunately, since this element is implemented in the generator relay, there are protection elements that will also respond to this event—notably the backup distance element. Therefore, we can make use of this element for built-in, additional dependability. We need to operate even for a sustained pickup of the backup distance element, since it is possible that an exciter problem could be coincident with an external fault. Fig. 7 shows the resulting logic.

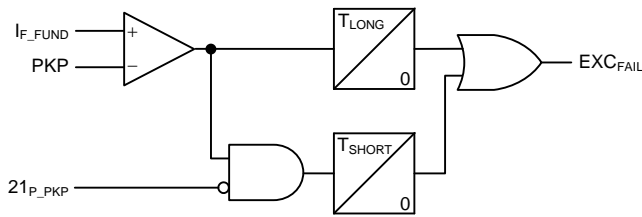


Fig. 7. Exciter failure detection logic.

D. Loss-of-Field Supervision

Protection against a loss-of-field (LOF) event has long been available for generators. An LOF event can produce a large in-flow of reactive power (VARs), thereby jeopardizing the voltage stability of the entire power system. It can also create stator end-core heating in a cylindrical rotor, which can quickly result in serious damage to the machine itself. Protection has generally been provided in the form of one or two offset mho elements. In this case, the inner zone is intended to operate for an LOF event when the machine is operating at close to rated load. The outer zone operates for LOF events closer to no load [5]. Fig. 8 shows an example application. Also shown are the generator capability curve (GCC), steady state stability limit (SSSL), and underexcitation limiter (UEL). Operation of the machine is restricted to the region outside the GCC. A secondary responsibility of the UEL is to prevent a false trip of the LOF protection. There are several criteria for setting the LOF protection function. Both zones should encompass the direct axis reactance (X_D), the transient reactance (X'_D), and the

SSSL and also be inside the UEL. Ideally, the SSSL should sit inside the inner zone. However, because the SSSL location depends on the system strength, this may not be possible. Since the LOF function is constructed from a phase-to-phase or positive-sequence mho element, there is a possibility that the LOF function could operate during power swings or out-of-step conditions if the apparent impedance enters the characteristic. As a consequence, both zones incorporate time delays to allow ride-through for stable power swings. It is typical to set the outer zone with a delay of 30 to 45 cycles and the inner zone to 15 cycles [6]. If the time delay is set too long, it is possible that a true LOF event could cause a loss of synchronism. This may result in the apparent impedance exiting the LOF mho characteristic during the slip before the LOF scheme times out. In this case, a failure to detect an LOF condition can occur [6].

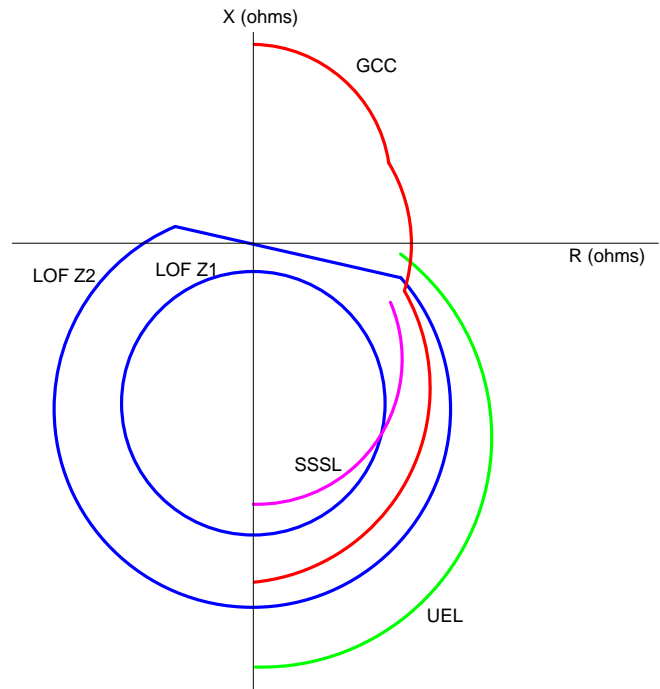


Fig. 8. Example LOF plot showing coordination with UEL, GCC, and SSSL [6].

Rather than using the traditional impedance-based scheme, it is possible to declare an LOF condition for low excitation voltage. However, this could fail to declare an LOF condition. For example, an open circuit between the exciter and rotor would result in an LOF event, but the field voltage that is measured at the exciter may otherwise be normal. Field voltage could, however, improve the effectiveness of the impedance-based scheme. Fig. 9 shows a simulation of a slow-clearing fault followed by a power swing. The automatic voltage regulator (AVR) is operational for this event. In this figure, the fault occurs at 0.3 seconds and is cleared at 0.5 seconds. The power swing develops on fault clearance as is evident by looking closely at the currents (I_a , I_b , I_c). Note that during a swing, the field current drops substantially, but the field voltage remains relatively high.

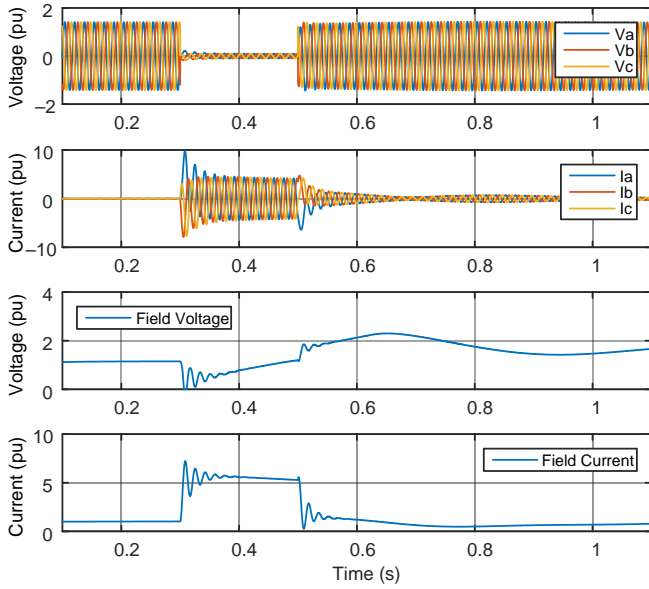


Fig. 9. Field voltage and current during a power swing.

We can conclude that if the impedance locus enters the LOF characteristic and the field voltage is high, then the event is more likely to be a power swing. If the field voltage is low, the event is more likely to be a true LOF event. This leads to the logic of Fig. 10.

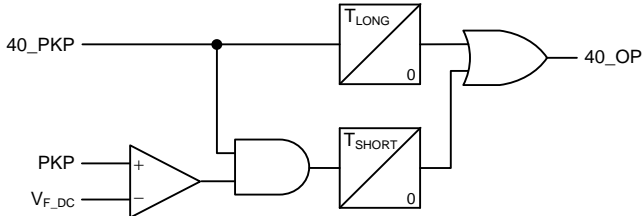


Fig. 10. LOF acceleration logic.

E. Generator Loss of Potential

Digital relays commonly employ terminal current and voltage measurements to detect a loss-of-potential (LOP) event. The premise of the scheme is as follows: a voltage change with a coincident change in current is a fault, but a voltage change without a coincident current change is an LOP condition. Complexities arise when the machine is offline, since there is no current flow at that time. LOP schemes usually discriminate between an offline LOP and a normal shutdown by looking at the rate of decay of positive-sequence voltage. Not all machines have the same behavior during shutdown. This may lead to spurious LOP assertion.

In the days of electromechanical (EM) generator protection, an LOP scheme was often implemented using a voltage balance relay. The relay compared two three-phase voltages, each from a different VT. This method has not been commonly employed in digital relays since it requires an increase in the number of voltage inputs.

During offline operation, the terminal voltage magnitude is equal to $I_{F_DC} \cdot X_D$ (product of the field current and direct axis reactance). We can therefore implement the equivalent of a voltage balance function as shown in Fig. 11. This logic

provides positive declaration of the loss of all three potentials.

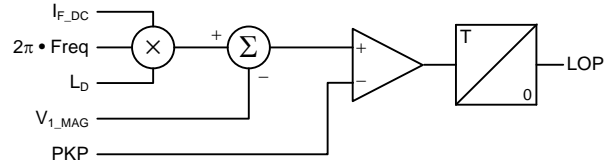


Fig. 11. LOP voltage balance logic using field current.

We can declare the loss of one or two potentials using the ratio of V_{2_MAG} over V_{1_MAG} . The scheme is intended for offline operation only. For online operations, apply the conventional voltage/current logic.

Since digital relays can track frequency over a wide range, the function will be effective for machines that operate at off-nominal frequencies during startup or shutdown. Due to the wide frequency range of this function, the logic uses the steady-state direct axis inductance (L_D).

III. DC GROUND-FAULT PROTECTION

Combustion gas turbines (CGT) differ from other types of generation in that the unit must be brought up to some percentage of rated speed before the turbine can begin to deliver power. Traditional CGT installations accelerated by mechanically coupling a starting (pony) motor or gas engine to the shaft of the machine. Fig. 12 shows an example of a simple open-cycle, single-shaft unit [7].

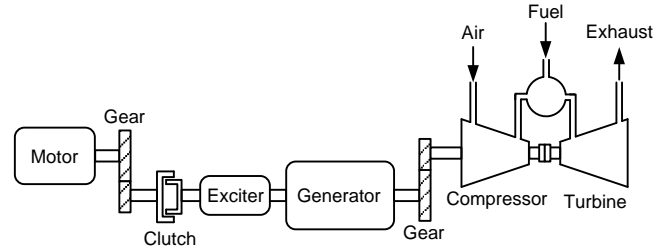


Fig. 12. CGT with a starting motor.

An alternative method, which has become increasingly more common, is known as static starting. This method uses the generator itself, operating as a motor, to bring the turbine up to speed [7]. Static starting typically uses a load commutated inverter (LCI) in order to precisely control the speed. Fig. 13 shows a simplified one-line diagram of this method.

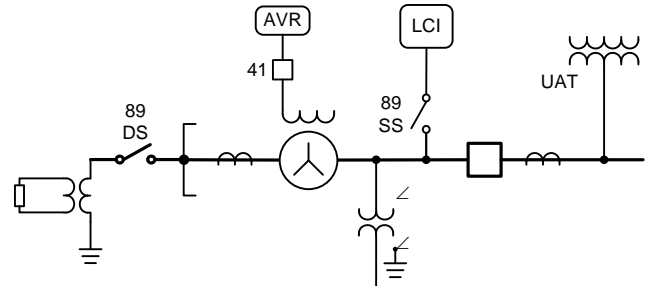


Fig. 13. CGT with static starting.

Fig. 14 shows a typical starting sequence. We can see that the machine operates at a low frequency (from 0 to 18 Hz) for a period of 10 to 15 minutes during purge and ignition and the associated acceleration and coast time periods. The machine slowly accelerates from approximately 10 Hz to its full speed over a period of about 15 minutes [7].

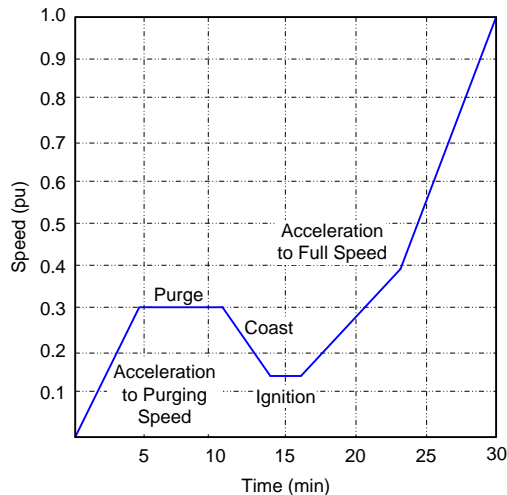


Fig. 14. Typical CGT starting sequence [7].

During startup, the starting switch, denoted as 89-SS in Fig. 13, is closed. If a ground fault develops on the dc link in the drive, the dc current flows through the grounding transformer and through a grounded-wye generator VT winding. This quickly drives the transformers into saturation. Overheating results from I^2R heating in the primary conductor and large eddy currents in each core.

One method to avoid dc ground-fault damage is to disconnect the generator neutral from ground during startup (via the 89-DS) and to use open-delta VTs at the generator terminals. An alternative approach is to employ dc ground-fault protection [8].

For a six-pulse converter, the dc link voltage is $6/\pi$ times the phase-to-phase voltage input to the LCI. The link voltage can be as high as 6,000 volts, depending on the particular generator. When a ground fault develops within the LCI, one-half of the dc link voltage appears at the LCI terminals. In the case of primary resistance grounding, the dc current at the generator neutral is limited by the neutral grounding resistor. If the generator is grounded through a neutral grounding transformer (NGT), then the current is limited only by the resistance of the NGT primary winding. Often, the generator VTs have series resistors that limit the fault current, so NGT damage is the limiting factor.

An RMS measurement, Fig. 15, includes both dc and any harmonic content in the current. Therefore, an RMS current measurement is the best indication of a thermal overload condition. A split-core, hall-effect CT provides an effective and unintrusive means to derive this signal.

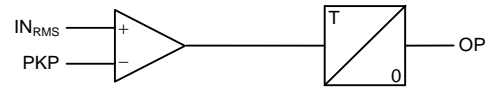


Fig. 15. DC ground-fault protection logic.

IV. SHAFT CURRENT

A. Cause of Shaft Voltage

The major cause of shaft voltage is due to stator core segmentation. The stator core of a large hydro machine is typically segmented to enable transportation of the stator core. This segmentation results in minor differences in flux around the stator. If the rotor poles align with the stator segment joints after a rotation of each pole pitch, the difference in flux will have an additive effect and generate a large shaft voltage and a large amount of energy. If the generator construction is such that rotor poles and the stator segments align after a rotation of one pole pitch, a much lower voltage and smaller amount of energy are generated in the shaft.

Tests performed at one power station (a hydro station in Australia), where brushes were added to the nondrive end of the generator and connected to ground, resulted in the shaft voltage dropping from 22 to 10 V while the shaft current was 390 A. 1 A at 1 V can cause pitting on the bearing face. This particular hydro station can generate a shaft voltage of up to 40 V. At another hydro station, the construction of the stator and rotor are such that the shaft voltage is on the order of 0.5 V, resulting in a lower shaft voltage and a smaller amount of energy.

B. Effects of Shaft Current on Bearings

Fig. 16 shows damage to a vertical hydro unit thrust bearing caused by shaft current. The shaft current caused metal to be removed from the white metal bearing face and to be dragged around the bearing face.



Fig. 16. Thrust bearing damage due to shaft currents (see striations in the bearing).

A closer inspection of the white metal bearing face, Fig. 17, shows pitting caused by arcing and the resulting abrasion of the bearing face. The associated guide bearing was also damaged.



Fig. 17. Enlargement showing damage to white metal thrust bearing.

C. Detection of Shaft Current

Monitoring the shaft voltage to determine shaft current is not effective. A low shaft voltage does not necessarily mean a low or nonexistent shaft current; significant shaft current can flow even if the shaft voltage is within an acceptable range. Monitoring shaft current is the best method to determine whether or not there is shaft current in the generator. Generator shaft current is typically composed of currents at different frequencies. The magnitudes and frequencies of these currents depend on the primary conditions of the power system and the generator's construction. When shaft current is present, it contains a dc component, a rotational speed component, a fundamental component, and harmonic components—particularly the third and ninth harmonics. On generators with a very small shaft voltage, the third harmonic current component present in the shaft current will also be low. Two common methods for measuring shaft current are a CT and a Rogowski coil.

1) Shaft CT

A Shaft CT is a toroidal CT with a large internal diameter that is mounted around the generator shaft. Unlike a normal CT installed on a power system, the measured current is between 1 and 10 A. The output current is between 1 and 3 mA. A typical installation uses a split-core CT in order to mount it around the generator shaft. Some manufacturers provide interleaved laminations at the split core joints so as to reduce iron losses. It is common to provide a test winding of two or three turns on the shaft CT to allow injection in the ampere range for testing purposes. This method also allows testing of the complete transformer circuitry.

Fig. 18 shows a shaft CT installed below a lower guide bearing on a vertical hydro generator shaft.



Fig. 18. Shaft CT mounted to a hydro generator; note that the mounting bracket does not fully enclose the CT.

As with any CT, the mounting brackets must not fully encircle the shaft CT, as this would create a shorted turn and corrupt the output of the CT. Due to variations of the flux within the area surrounding the shaft CT, the CT could produce a current even if no shaft current is flowing. Despite the CT producing an output with no shaft current present, this is a simple method for measuring and detecting shaft currents. Due to the low current output of the CT, any device monitoring this current must be capable of processing a milliampere input signal. The monitoring device should have the option to operate on either the fundamental current component or the third harmonic current component. We can use the third harmonic current component to provide a more sensitive detection for generators that produce a larger shaft voltage and current.

Fig. 19 shows the frequency spectrum for a shaft current of 2 A primary. This particular generator is capable of generating a shaft voltage of 20 V.

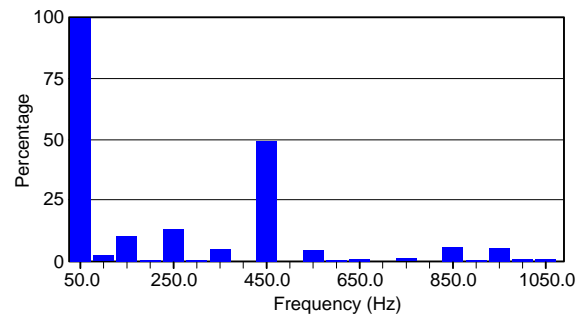


Fig. 19. Frequency spectrum of the shaft current due to a 2 A primary fault current.

However, for this particular generator, due to stator flux variation along the stator core, the shaft CT can produce an output current when no actual shaft current is flowing. Fig. 20 shows a frequency spectrum of the current output from the shaft CT.

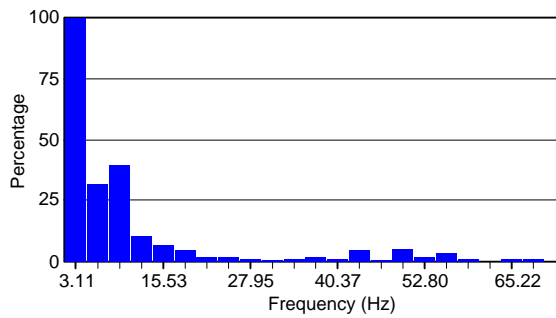


Fig. 20. Frequency spectrum of the output current of the shaft CT when no shaft current is present and the output current is due to uneven stator flux distribution.

Without an actual shaft current present, the frequency spectrum of the shaft CT output current contains a higher rotational component and a lower third-harmonic current component. In summary, if the machine generates a large shaft voltage and if the third-harmonic content exceeds the threshold, we can trip. If there is a low shaft voltage and we monitor the shaft current using the fundamental current, we can only alarm.

2) Rogowski Coil

An alternative method of measuring the shaft current uses a Rogowski coil. The advantage of using a Rogowski coil is that it is flexible and easier to mount than a shaft CT. The Rogowski coil is installed around the shaft, and for duplicate protection, it can be mounted below a shaft CT if fitted as shown in Fig. 21. As with the shaft CT, the Rogowski coil cannot be installed with a metal mounting bracket that encloses the coil, as this would create a shorted turn around the Rogowski coil.

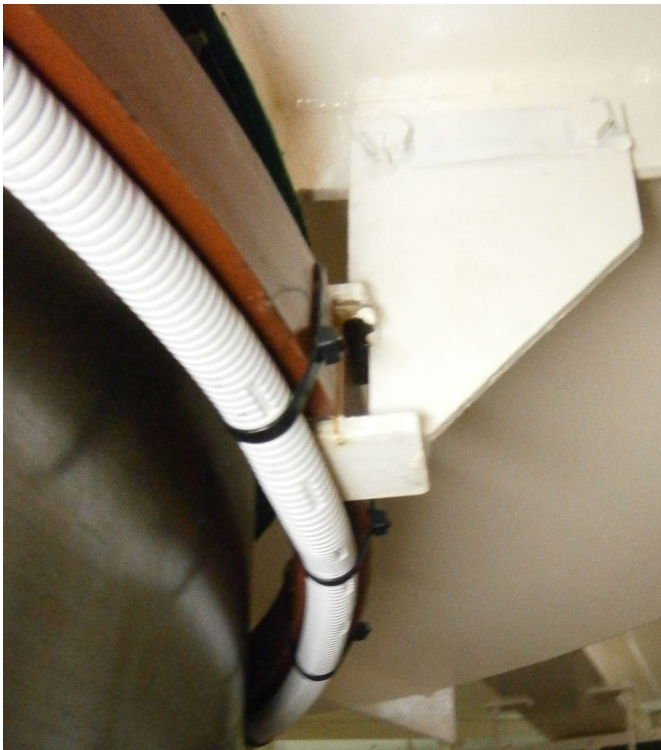


Fig. 21. Mounting of a Rogowski coil for use as a shaft current monitor.

The integrator range of the Rogowski coil needs to match the intended primary current. In normal Rogowski coil installations, the input range to the integrator may have ranges of tens of thousands of amperes; however, shaft current installations require a very low input current value. For shaft current applications, these integrators typically provide an output voltage of 0.5 V for 1 A of primary shaft current. Injecting a lower primary current into the integrator is generally not possible, as the integrator gain required at lower currents encroaches on the noise levels of the integrator circuitry. Depending on the integrator, the output can be either a time-varying instantaneous voltage value or a dc RMS voltage value; milliampere outputs are also available. If the output of the integrator is connected to a protective device, it is better that the output be time based rather than the RMS equivalent. This will allow the device to provide protection or detection using the fundamental or third harmonic component. A test winding, as shown in Fig. 22, can also be provided by installing a single turn around the Rogowski coil and connecting it to a set of terminals. Under normal operating conditions, these terminals are left in an open-circuit state.



Fig. 22. A Rogowski coil with a test winding.

Fig. 23 shows the frequency spectrum of the output voltage for a 2 A primary shaft CT. This particular generator is capable of developing a shaft voltage of 20 V. However, on this particular generator, the Rogowski coil can develop an output voltage with no actual shaft current flowing, despite the fact that there is a single wire return within the Rogowski coil.

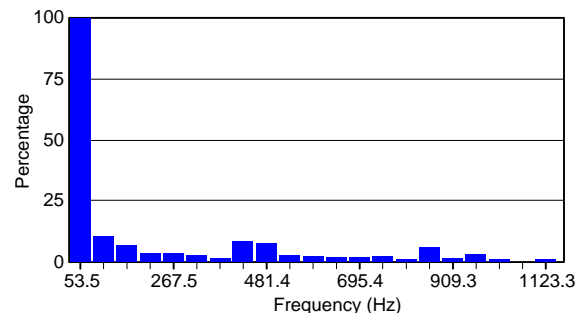


Fig. 23. Frequency spectrum of the shaft current due to a 2 A primary fault current.

The system is configured to detect 1 A in the shaft while there is up to 12,000 A of stator current adjacent to the Rogowski coil. There is a large amount of stray flux near the Rogowski coil, and it is nearly impossible to reject all of it. Fig. 24 shows the frequency spectrum output of a Rogowski coil when no actual shaft current is flowing. Fig. 25 is the frequency spectrum of the shaft voltage when no shaft current is flowing.

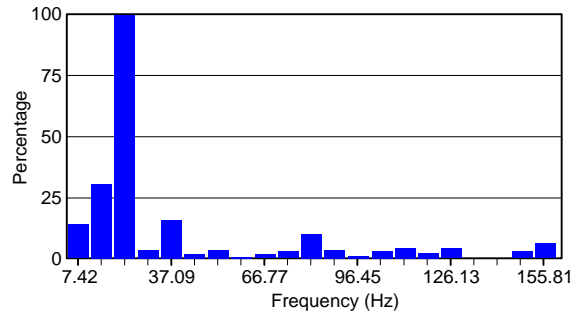


Fig. 24. The frequency spectrum output from a Rogowski coil when no actual shaft current is flowing.

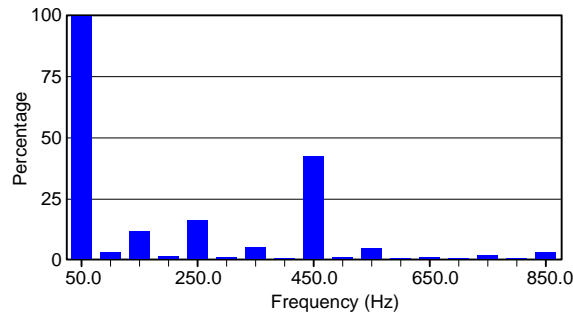


Fig. 25. The voltage frequency spectrum when no actual shaft current is flowing.

Shaft current typically flows between the bearings of the hydro generator. To prevent shaft current from flowing through the bearings, the turbine end of the shaft is grounded and the bearings on the rotor end are insulated as Fig. 26 shows.

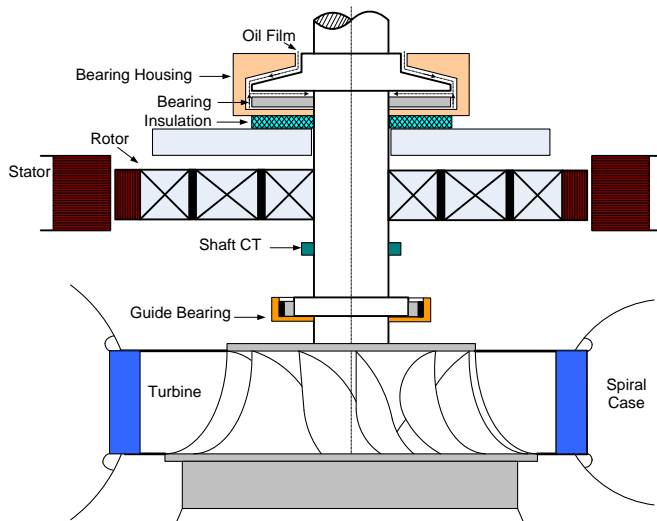


Fig. 26. Simple sketch of a hydro generator indicating the location of the insulated bearing and the shaft ground.

The insulation includes the piping for the jacking oil pumps, the instrumentation cable sheathing, and the mounting bolts. The shaft current monitor can be installed anywhere below the insulated bearing(s).

V. STATOR FIELD DIFFERENTIAL

We begin this discussion with a brief overview of traditional schemes for protection of the stator winding. The information contained in this section has previously been discussed in [9] and [10] and is reproduced here for the reader's convenience. Differential protection is one of the main protection elements responsible for detecting internal generator faults. Generator differential protection schemes are designed to detect faults by comparison of current flowing into and out of the stator. A variety of schemes are possible [9].

A. Self-Balancing Differential

In this scheme, shown in Fig. 27, the overcurrent elements are connected to core-balance CTs on a per phase basis. This allows for detecting both phase and ground faults.

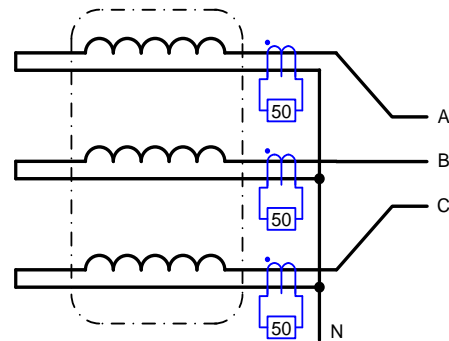


Fig. 27. Self-balancing differential protection scheme.

This scheme allows for low-ratio CTs to be applied, making it very sensitive and secure for external faults. However, saturation for internal faults is possible if the CT burden is too high. One drawback of this scheme is that both ends of the winding must pass through the windows of the core-balance CT, making this scheme difficult to apply on large machines. In addition, these CTs are susceptible to stray flux from nearby current-carrying conductors. This places some sensitivity limitations on this scheme. Defining $I_{pkp_{SB}}$ as the minimum pickup setting of the overcurrent element and CTR_{CB} as the CT ratio of the core-balance CT, the sensitivity of this scheme can be calculated by (2).

$$I_{min_{SB}} = CTR_{CB} \cdot I_{pkp_{SB}} \quad (2)$$

B. Biased Differential

This scheme, as shown in Fig. 28, makes use of CTs on both sides of the winding on a per phase basis. The CTs are sized to carry the total generator current. On low-impedance-grounded machines, this scheme can detect phase-to-phase, phase-to-ground, and three-phase faults, but on high-impedance-grounded machines, it is not effective for phase-to-ground faults. For security, a biasing method is used that requires the differential current (O_P) to be greater than a

percentage of the restraint current ($K_{PH} \cdot R_{ST}$). This results in the well-known slope characteristic when the differential current is plotted against the restraint current. The restraint current is typically the scalar sum of the currents on each side of the zone (R_{ST}). This scheme employs a variety of characteristics, including variable slope, dual slope, and adaptive slope.

Defining K_{PH} as the slope setting of the differential element and CTR_{PH} as the CT ratio of the primary CT and assuming that the machine carries rated load, the sensitivity of this scheme is approximated by (3).

$$I_{min_{PH}} \cong CTR_{PH} \cdot K_{PH} \cdot I_{G_{RATED}} \quad (3)$$

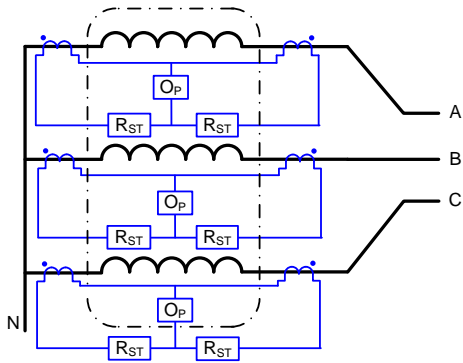


Fig. 28. Biased differential protection scheme.

C. High-Impedance Differential

As can be seen from Fig. 29, this scheme is similar to the biased differential scheme in that it makes use of CTs on both sides of the winding on a per phase basis. The CTs are connected in parallel via an overcurrent element in series with the large resistor. This connection creates a high-impedance path between the CT terminals, hence its name.

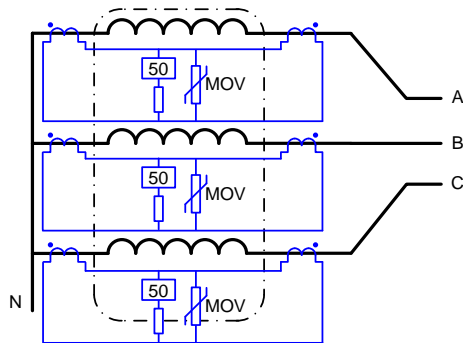


Fig. 29. High-impedance differential protection scheme.

This scheme is extremely secure for external faults in the presence of CT saturation. This scheme is generally more sensitive than the biased differential element, because the high impedance in series with the operating coil allows the scheme to be set according to the voltage drop across the resistor. Some schemes have a pickup current as low as 20 mA. The main disadvantages of this scheme are that it requires dedicated CTs and the CTs on either side of the winding must have matching characteristics. For this reason, multifunction relays that perform generator protection generally incorporate biased differential protection elements.

Another disadvantage is the fact that a shorted CT disables the scheme. A variation of this scheme uses a single overcurrent element for restricted earth fault detection on low-impedance-grounded machines.

Defining $I_{pk_{PHZ}}$ as the operating current of the overcurrent element and neglecting CT excitation current and MOV current, the sensitivity of this scheme is approximated by (4).

$$I_{min_{PH}} \cong CTR_{PH} \cdot I_{pk_{PHZ}} \quad (4)$$

D. Stator-Rotor Differential Elements

The three differential schemes mentioned previously in this section are optimized to detect shunt faults in a generator; however, none of these schemes are optimized to detect series faults such as a turn-to-turn fault in either the rotor or stator windings of the generator. The reason for this is that the previous schemes measure the net current flow in a winding. A turn-to-turn fault is a series fault (part of the winding is shorted), which results in the current flowing into the winding being equal to the current flowing out of the winding so that the net differential phase current is zero. Since the previous schemes measure the net current flow in a winding, these will not detect a turn-to-turn fault. So how do you detect a turn-to-turn fault using a differential element?

Let us step back a moment and look at a transformer. We know that a turn-to-turn fault in a transformer is going to upset the ampere turns (AT) balance of that transformer and result in negative-sequence current flowing into the transformer. Negative-sequence current always flows toward the fault point. Therefore, by measuring the net negative-sequence flow into a transformer, we can detect a turn-to-turn flow in a transformer [11].

Let's consider a generator as a three-winding rotating transformer, with the stator winding (for simplicity) being one winding, the rotor (field) winding being the second winding, and the damper winding being the third winding, and apply the same reasoning as we did for a transformer. We can now provide turn-to-turn fault protection for a generator by applying the AT balance to the equivalent three-winding transformer as shown in Fig. 30a [10].

The negative-sequence current in the stator winding develops a magnetic field that rotates in the opposite direction of the rotor. As a result, the negative-sequence current in the stator winding is going to induce a double-frequency current in the field and damper windings of the rotor. It is possible to extract the negative-sequence current from the field winding but not from the damper winding (it is not possible to measure the current in the damper winding). However, we can overcome this hurdle by converting the impedances of the field and damper windings to the same voltage base and connecting the two impedances in parallel to one another. This forms one equivalent winding, as shown in Fig. 30b [10]. Forming one equivalent winding allows us to reduce the three-winding transformer to a two-winding transformer. Typically, the exciter does not generate any double-frequency voltage, so we can view the field winding as being shorted with a total impedance of Z_{FT} . The damper winding having a leakage impedance of Z_D , as shown in Fig. 30b, implies that

we can apply the AT balance principle to detect a turn-to-turn fault.

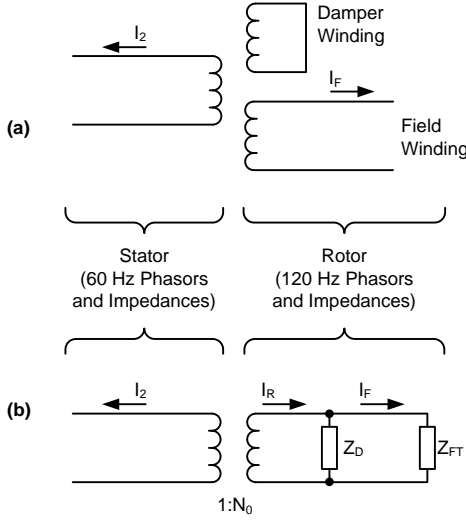


Fig. 30. An equivalent three-winding transformer relating the negative-sequence stator current and the double-frequency components of the field and damper currents (a) and a two-winding equivalent representation with the field and damper windings brought to the same voltage base (b).

We know that we can only measure the negative-sequence current in the stator (I_2) and the double-frequency current in the field winding (I_F) (we cannot measure the double-frequency current in the damper winding). Knowing this, we can calculate the total double-frequency current in the rotor as follows:

$$I_R = I_F \cdot \left(1 + \frac{Z_{FT}}{Z_D}\right) \quad (5)$$

Assuming that the turn's ratio of the two-winding equivalent transformer is N_0 , the AT balance for any external unbalance with the generator in a healthy state can now be written as:

$$I_2 = N_0 \cdot I_R = N_0 \cdot I_F \cdot \left(1 + \frac{Z_{FT}}{Z_D}\right) \quad (6)$$

Therefore, for any external unbalance, the ratio of the negative-sequence stator current (I_2) and the double-frequency rotor current (I_F) for a healthy machine is a constant and can be written as:

$$N_{SF} = \frac{I_2}{I_F} = N_0 \cdot \left(1 + \frac{Z_{FT}}{Z_D}\right) \quad (7)$$

where N_{SF} is the effective turns ratio between the stator winding and the field winding. A turn-to-turn fault will upset the AT balance condition described by (6) and (7) allowing detection of the turn-to-turn fault.

1) Stator-Rotor Current Unbalance (60SF) Element

Based on the principle derived above, we propose a new protection element, the stator-rotor current unbalance element (60SF). This element is not only capable of detecting turn-to-turn faults in the generator, but it can also be used to detect phase-to-ground faults in the stator winding. The element measures the stator current and from this derives the

negative-sequence current magnitude. It measures the field current (using a shunt or Hall Effect sensor) and from this extracts the double-frequency current component. A simple implementation of how the element currents are derived is shown in Fig. 31.

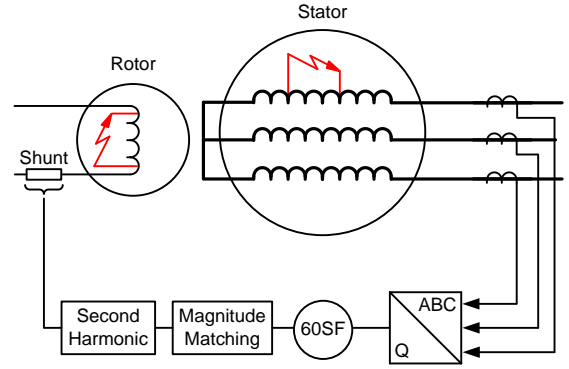


Fig. 31. The 60SF turn-to-turn fault protection element for synchronous generators.

The 60SF element uses the effective transformation ratio (N_{SF}) to match magnitudes and verify if the two current magnitudes balance. A simple implementation of the 60SF element design is done using a percentage differential, where the operating signal is obtained by (8) and the restraining signal is obtained by (9).

$$I_{OP} = \left| |I_{2(60\text{ Hz})}| - N_{SF} \cdot |I_{F(120\text{ Hz})}| \right| \quad (8)$$

$$I_{RST} = \left| |I_{2(60\text{ Hz})}| + N_{SF} \cdot |I_{F(120\text{ Hz})}| \right| \quad (9)$$

Comparing the operating and the restraining signals using a slope setting of 20 percent for a percentage differential scheme results in an operating characteristic shown by the green lines in Fig. 32. The results shown in Fig. 32 were obtained by testing a 200 MVA machine model in a Real Time Digital Simulator[®] (RTDS) at various loading conditions (50 MW and 200 MW) and with turn-to-turn faults involving a different percentage of the winding.

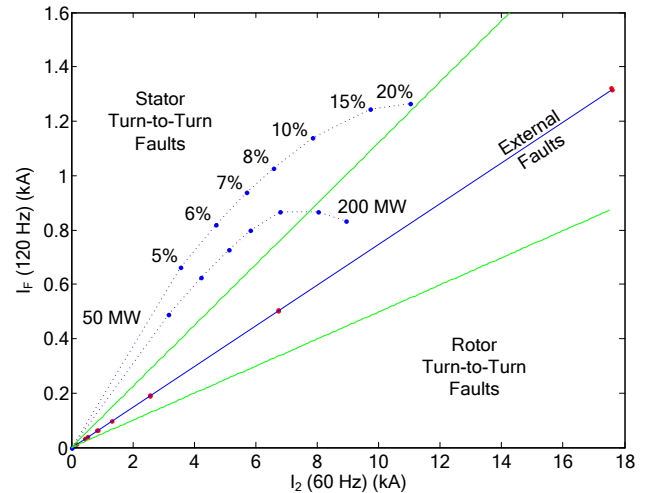


Fig. 32. Negative-sequence stator current magnitude vs. double-frequency field current magnitude for both external faults (red dots) and internal turn-to-turn faults (blue dots) in a 200 MW generator.

A second type of stator-rotor differential element that makes use not only of the current magnitudes but also their phases (87SF) is described in [10]. The 87SF offers greater sensitivity when compared to the 60SF, but both elements have the ability to detect turn-to-turn faults in a generator.

VI. GENERATOR CONTROL MONITORING

Time-stamping of generating station data can be very useful for monitoring and validating various generator control system performances. The generating station data can be terminal voltages, terminal currents, speed, rotor angle, active power, field voltage, field current, temperature, hydrogen pressure, etc. [12]. Synchrophasors provide a mechanism to time stamp the generator data and make them readily available for online and offline control system monitoring applications like generator model validation, automatic voltage regulator (AVR) or excitation control system performance, power system stabilizer (PSS) tuning and performance, and governor control tuning and performance. Phasor measurement units (PMU) or protective relays with PMU functionality create synchrophasor data. A synchrophasor data packet consists of voltage and current phasors and analog and digital data. PMUs calculate synchronized phasors from conventional data such as terminal voltages and currents and reference them to absolute time (UTC). Nonconventional data, such as field voltage, active power, rotor angle, and speed, can be time-stamped and included in the analog data section of the synchrophasor data packet. The IEEE C37.118 standard requires that the phasors included in the synchrophasor data packet be corrected for filtering and processing delays. But the standard does not provide any guidelines for delay correction of analog data included in the synchrophasor data packet. If you are using nonconventional analog data in a synchrophasor packet, then ensure you minimize the acquisition delay.

Apart from controlling the generator output voltage, a generator excitation system plays a key role in stabilizing the generator and the connected power system during transient disturbances. The main components of a generator excitation system are the AVR and PSS as shown in Fig. 33 [13].

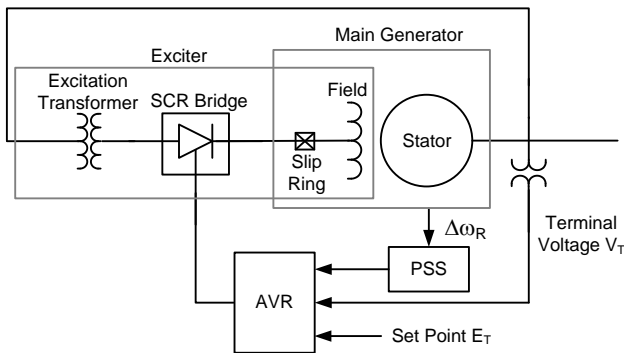


Fig. 33. Generator excitation system.

The primary objective of the AVR is to regulate the generator voltage to the specified set point. The generator protective functions such as underexcitation, overexcitation, and volts per hertz are also included in the AVR as set points

and limits. The primary objective of the PSS is to damp out power system oscillations. The PSS measures change in the synchronous speed of the generator and injects it to the AVR. The PSS damps out the negative effects of a fast-acting AVR. System operators rely on the accurate representation of the generator excitation system for transient and small signal stability studies. In North America, NERC requires a generator owner to validate the generator excitation model periodically [14]. After a transient event, system operators can readily use synchrophasor data obtained during the transient to validate their excitation model. Generator owners can also use synchrophasor data for excitation system testing and model validation when the unit is offline [15]. Synchrophasor data can also be used to efficiently commission a PSS while the unit is online [16].

Monitoring the performance of a generator control system is critical. Synchrophasor data measured at the generating station can be used to monitor the health and performance of the exciter, AVR, PSS, and governor. A malfunctioning generator AVR caused undesirable oscillations in the New York Independent System Operator (NYISO) region in May 2013 [17]. Similarly, a malfunctioning generator PSS also caused oscillations in May 2013. These two events were detected at the transmission level by system operators using synchrophasor data. These could have been detected at the generating station itself.

VII. SUBSYNCHRONOUS RESONANCE MONITORING

Series capacitors provide an economic way to increase the power transfer capabilities of existing power system transmission lines. If a fault occurs on a series-compensated power system, off-nominal frequencies are generated. If one of these frequencies coincides with one of the resonant frequencies of the turbine, a subsynchronous resonance (SSR) condition occurs. SSR refers to the phenomenon in which the electrical power system exchanges energy with the mechanical system of the turbine generators at one or more frequencies below the synchronous frequency of the power system [18]. While there are other forms of SSR interaction, this paper only discusses the aforementioned phenomenon.

For steady-state studies, the turbine generator is usually considered as a single mass rotating at a synchronous speed. However, when doing SSR studies, the generator and turbine need to be modeled as separate rotating masses (finite inertia segments) e.g., high-pressure turbine, low-pressure turbine, generator, exciter, etc. A spring constant and a damping coefficient represent the average shaft material behavior between the masses, as shown in Fig. 34.

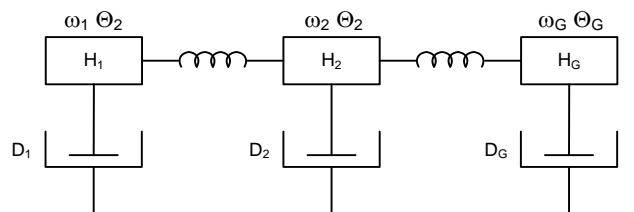


Fig. 34. Spring-mass S model for a multimass shaft system.

The motion of the different masses is described by a set of equations according to Hooke's law of material deformation and Newton's law of mechanics [18]. These equations are a set of first order differential equations. They exhibit several natural frequencies or modes of torsional vibration, and the shaft system responds to the applied torque with oscillations in each mode.

If one of the modes is excited by an electrical oscillation and the eigenvalue associated with this mode has a positive real part, then the generated electrical torque will oscillate with the mechanical system and amplify itself. Relative movements between the masses, as indicated by the shape of the right eigenvector, generate a large amount of torque, causing a loss-of-life of the shaft, if the shaft is not damaged outright. The generator should not be allowed to go through undamped subsynchronous oscillations because these can cause significant economic loss.

A. Challenges for SSR Detection

Even though real-world SSR events are rare, their consequences are very severe. Over the years, various SSR detection relays have been developed as the last defense for generators that can experience an SSR condition. For generators located in areas where SSR has a low probability of occurrence, an SSR relay is usually the only protection against an SSR condition [19]. Most of these relays use electrical input signals such as terminal voltages and currents.

Challenges of designing a practical SSR relay include low amplitude of sustained or growing subsynchronous-frequency currents, low-frequency range, rapid response time requirement to reduce damage, high-amplitude fault currents, and the requirements to not false trip.

B. Analysis of the SSR Phenomenon Using IEEE Second Benchmark Model

To analyze the phenomenon behavior and develop countermeasures, an IEEE working group on SSR developed the first benchmark model in 1977. This provides the simplest possible model: a turbine generator connected to a single radial series-compensated line. However, this configuration is rarely encountered in real power system operations. In 1985, the second benchmark model for SSR study was published and was more realistic [19]. In this study, the IEEE second benchmark model on SSR is built in the RTDS. The one-line diagram is shown in Fig. 35. With the electrical data and the shaft parameters described in [19], modal frequencies can be calculated as shown in Table I. From the eigenvalue analysis results of the simulated power system, Mode 1 is the unstable mode [19].

TABLE I
MODAL QUANTITIES

Mode	f_N	λ_N^\dagger	H_N^\ddagger
1	24.65 Hz	0.05 rad/s	1.55 pu
2	32.39 Hz	0.05 rad/s	9.39 pu
3	51.10 Hz	0.05 rad/s	74.80 pu

[†] λ_N is the calculated damping factor of each mode.

[‡] H_N is the inertia in modal domain.

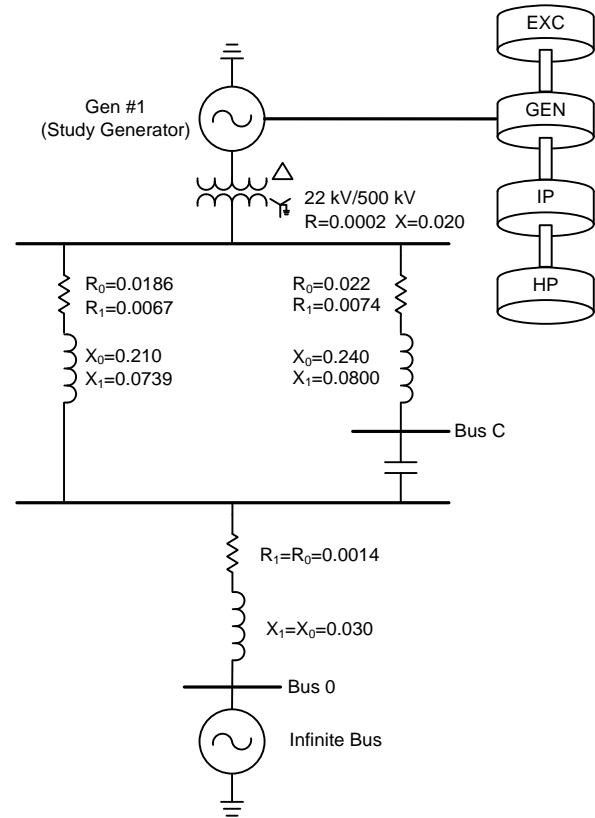


Fig. 35. IEEE second benchmark model on SSR [19].

A three-phase fault was initiated on the high-voltage side of the transformer and then cleared. Fig. 36 shows the torque generated between two sets of points on the generator shafts (the generator shaft segment between the generator and the low-pressure turbine, and the segment between the high-pressure turbine and low-pressure turbine) and the velocity of the masses after the disturbance for a three-phase fault with a clearing time of 0.0167 s. Note that a temporary fault lasting for 0.0167 s was simulated in this study to show the torque amplification problem caused by SSR. In reality, fault clearing time will be longer than 0.0167 s.

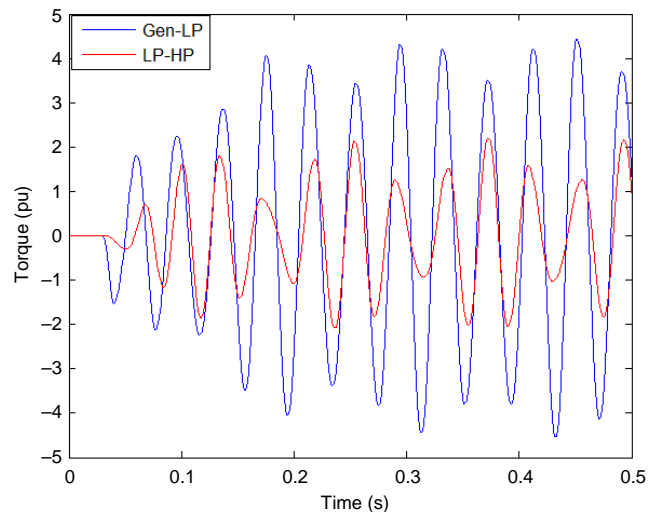


Fig. 36. Shaft torque response for a three-phase fault with a fault clearing time of 0.0167 s.

Fig. 36 shows the torque amplification phenomenon. The peak torque between the generator and low-pressure turbine is at approximately 4.02 pu. Fig. 37 shows the generator terminal current and voltage signals and the speed signals of the four masses.

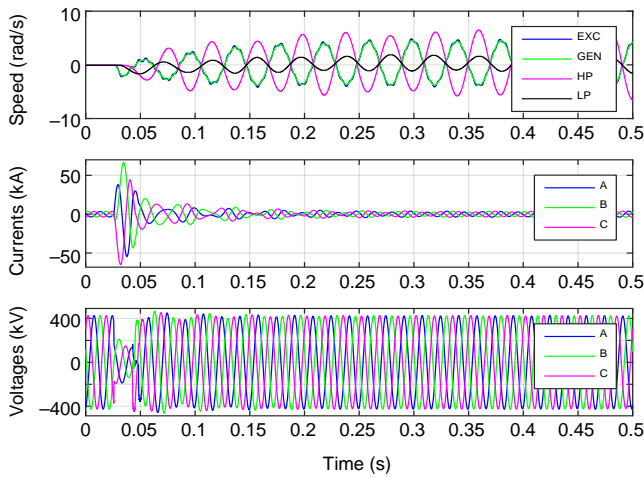


Fig. 37. Generator terminal current and voltage signals and the speed signals of the four masses.

From the speed signals, we see that the exciter, generator, and the high-pressure turbine have different velocity deviations, which result in the abnormally high torques on the shafts. We used a Discrete Fourier Transform (DFT) to analyze the frequency components of the above signals. Fig. 38 shows the result for the high-pressure turbine speed, the A-phase terminal current, and the A-phase terminal voltage. It must be noted that, in reality, the speed signals may not be available at all of the turbines. The speed of the turbines is usually measured by transducers mounted adjacent to the toothed wheel on the machine shaft. When compared using simulation data, these signals have more limited resolution and quality compared with terminal measurements.

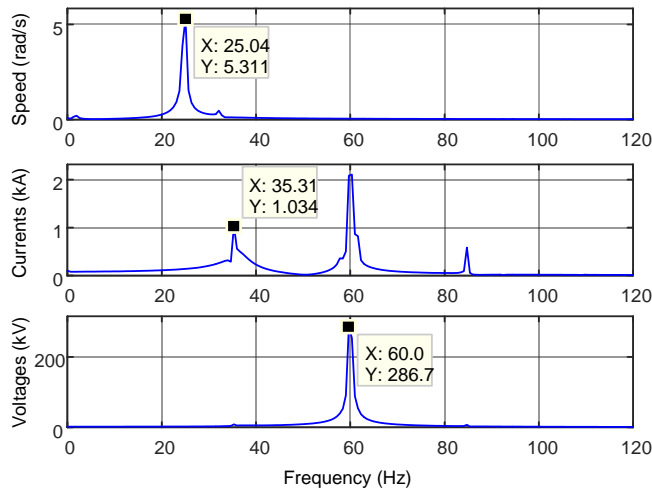


Fig. 38. DFT results for high-pressure turbine, A-phase terminal current, and A-phase terminal voltage.

From the above results, we observe a noticeable subsynchronous-frequency range component in the generator

terminal current, while the signal is much less noticeable in the voltage. Since the subsynchronous range current signals are present together with the fundamental frequency signals, it is challenging to separate these signals rapidly and accurately. Generator speed is the most direct way to detect SSR. Under normal operation, the shafts will rotate at a synchronous speed. With the SSR excited, the shaft will oscillate at the unstable mode on top of the synchronous speed. It is relatively easy to extract the subsynchronous-frequency component from the speed signal and therefore facilitates identifying SSR faster and more accurately. For this reason, it is advisable to install a speed transducer on the generator shaft.

VIII. CONCLUSIONS

This paper has shown that by making use of additional generator measurements, such as field current and voltage, and applying the appropriate filtering, these measurements can be used to complement traditional voltage and current measurements, resulting in better generator protection. These additional measurements can be used to monitor the generator more effectively. Therefore, by adding these measurements to our generator protection and monitoring scheme, we effectively increase the level of observability of the generator, which in turn allows us to operate our generator for longer periods of time more economically and efficiently.

IX. REFERENCES

- [1] IEEE Standards Dictionary. Available: <http://ieeexplore.ieee.org/xpls/dictionary.jsp>.
- [2] IEEE C37.102-2006, IEEE Guide for AC Generator Protection.
- [3] IEEE Standard 67-2005, IEEE Guide for Operation and Maintenance of Turbine Generators.
- [4] C. J. Mozina, et al., "Coordination of Generator Protection with Generator Excitation Control and Generator Capability," Working Group J-5 of the Rotating Machinery Subcommittee, Power System Relay Committee," Power Engineering Society General Meeting, 2007. IEEE, Tampa, FL, 2007, pp. 1-17.
- [5] D. Riemert, *Protective Relaying for Power Generation Systems*. CRC Press, December 2005.
- [6] NERC Standard PRC-019-2 – Coordination of Generating Unit or Plant Capabilities, Voltage Regulating Controls, and Protection. Available: <http://www.nerc.com>.
- [7] W. B. Boym, R. W. Ferguson, and J. G. Partlow, "Methods of Starting Gas-Turbine-Generator Units," *Transactions of the AIEE*, Vol. 73, Issue 1, January 1954.
- [8] Working Group J-2 of the Rotating Machinery Subcommittee, "Protection Considerations for Combustion Gas Turbine Static Starting," IEEE Power System Relaying Committee. Available: http://pes-psrc.org/Reports/J2_ProtectionConsiderationsforCGTStaticStarting%20Final2.pdf.
- [9] D. Finney, N. Fischer, and D. Taylor, "How to Determine the Effectiveness of Generator Differential Protection," proceedings of the 40th Annual Western Protective Relay Conference, Spokane, WA, October 2013.
- [10] B. Kasztenny, N. Fischer, and H. J. Altuve, "Negative-Sequence Differential Protection—Principles, Sensitivity, and Security," proceedings of the 41st Annual Western Protection Conference, Spokane, WA, October 2014.
- [11] J. Mraz, J. Pomeranz, and J. D. Law, "Limits of Sensitivity for Detecting Inter-turn Faults in an Energized Power Transformer,"

proceedings of the 34th Annual Western Protective Relay Conference, Spokane, WA, October 2007.

- [12] N. Fischer, G. Benmouyal, S. Samineni, "Tutorial on the Impact of the Synchronous Generator Model on Protection Studies," proceedings of the 35th Annual Western Protective Relay Conference, Spokane, WA, October 2008.
- [13] NASPI Technical Report, "Diagnosing Equipment Health and Misoperations With PMU Data," March 20, 2015. Available: <https://www.naspi.org/File.aspx?fileID=1417>.
- [14] Working Group 10 of the Electric Machinery Committee, "IEEE Guide for Online Monitoring of Large Synchronous Generators," IEEE Power and Energy Society, 2014. Available: <https://standards.ieee.org/findstds/standard/1129-2014.html>.
- [15] C. J. Mozina, "Implementing NERC Guidelines for Coordinating Generator and Transmission Protection," proceedings of the 65th Annual Conference for Protective Relay Engineers, College Station, TX, April 2012, pp. 491–504.
- [16] J. C. Agee, S. Patterson, J. Seitz, "Excitation System Testing and Model Validation," Power Engineering Society 1999 Winter Meeting, IEEE, New York, NY, 1999, pp. 177–181 Vol. 1.
- [17] W. Gu, "Commissioning Generator AVR, PSS and Model Validation," IEEE 28th Canadian Conference on Electrical and Computer Engineering, Halifax, NS, 2015, pp. 669–673.
- [18] P. M. Anderson, B. L. Agrawal, J. E. Van Ness, *Subsynchronous Resonance in Power Systems*, IEEE Power Engineering Society, New York: IEEE Press, 1990.
- [19] "Second Benchmark Model for Computer Simulation of Subsynchronous Resonance," IEEE Transactions on Power Apparatus and Systems, Vol. PAS-104, No. 5, pp. 1057–1066, May 1985.

X. BIOGRAPHIES

Terry Foxcroft has worked in the power industry for over 36 years. He has worked in the protection, commissioning, testing, and design fields for over 30 years. He has presented papers at many national and international conferences. Terry is also a member of the Australian CIGRE B5 Committee. Terry is responsible for protection design at Snowy Hydro.

Normann Fischer received a Higher Diploma in Technology, with honors, from Technikon Witwatersrand, Johannesburg, South Africa, in 1988; a BSEE, with honors, from the University of Cape Town in 1993; an MSEE from the University of Idaho in 2005; and a PhD from the University of Idaho in 2014. He joined Eskom as a protection technician in 1984 and was a senior design engineer in the Eskom protection design department for three years. He then joined IST Energy as a senior design engineer in 1996. In 1999, Normann joined Schweitzer Engineering Laboratories, Inc., where he is currently a fellow engineer in the research and development division. He was a registered professional engineer in South Africa and a member of the South African Institute of Electrical Engineers. He is currently a senior member of IEEE and a member of the American Society for Engineering Education (ASEE).

Dale Finney received his bachelor of engineering degree from Lakehead University and his master of engineering degree from the University of Toronto. He began his career with Ontario Hydro, where he worked as a protection and control engineer. Currently, Mr. Finney is employed as a senior power engineer with Schweitzer Engineering Laboratories, Inc. His areas of interest include generator protection, line protection, and substation automation. Mr. Finney holds several patents and has authored more than 20 papers in the area of power system protection. He is a member of the main committee and the rotating machinery subcommittee of the IEEE PSRC. He is a senior member of the IEEE and a registered professional engineer in the province of Nova Scotia.

Satish Samineni received his bachelor of engineering degree in electrical and electronics engineering from Andhra University, Visakhapatnam, India, in 2000. He received his master's degree in electrical engineering from the University of Idaho in 2003. Since 2003, he has been with Schweitzer Engineering Laboratories, Inc. in Pullman, Washington, where he is a senior power engineer in the research and development division. He has authored or coauthored several technical papers and holds a United States patent. His

research interests include power electronics and drives, power system protection, synchrophasor-based control applications, and power system stability. He is a registered professional engineer in the state of Washington and a senior member of IEEE.

Yu Xia received his BS from the University of Science and Technology of China, Hefei, Anhui, China in 2008 and his PhD from the University of Idaho in 2013. He joined Schweitzer Engineering Laboratories, Inc. in 2011 and holds the position of power engineer in the research and development division. He is pursuing an MBA degree from the Stern School of Business at the New York University. He is a member of the IEEE Power & Energy Society.